International Journal of Mass Spectrometry 285 (2009) 31–41

Contents lists available at ScienceDirect

International Journal of Mass Spectrometry

journal homepage: www.elsevier.com/locate/ijms

Flowing afterglow selected ion flow tube (FA-SIFT) study of ion/molecule reactions in support of the detection of biogenic alcohols by medium-pressure chemical ionization mass spectrometry techniques

F. Dhooghe [a,b], C. Amelynck [a,*], J. Rimetz-Planchon [a], N. Schoon [a], F. Vanhaecke [b]

[a] Belgian Institute for Space Aeronomy, Ringlaan 3, B-1180 Brussels, Belgium
[b] Department of Analytical Chemistry, Ghent University, Krijgslaan 281, S12, B-9000 Ghent, Belgium

ARTICLE INFO

Article history:
Received 16 December 2008
Received in revised form 1 April 2009
Accepted 2 April 2009
Available online 10 April 2009

Keywords:
FA-SIFT
CIMS
Ion/molecule reactions
Biogenic alcohol

ABSTRACT

This article deals with the validation of and first measurements with a newly constructed flowing afterglow selected ion flow tube (FA-SIFT) instrument. All reactions were studied in He buffer gas at a pressure of 1.43 hPa and a temperature of 298 K.

The validation consisted of the study of the gas-phase ion/molecule reactions of methanol and ethanol (M) with the reactant ions $H_3O^+\cdot(H_2O)_n$ (n = 0–3), MH^+, M_2H^+, and $MH^+\cdot H_2O$ and the reactions of MH^+ with H_2O. Obtained results are compared with available literature data and with calculated collision rate constants.

The validated FA-SIFT has subsequently been used to characterize the reactions of the unsaturated biogenic alcohols 2-methyl-3-buten-2-ol, 1-penten-3-ol, *cis*-3-hexen-1-ol and *trans*-2-hexen-1-ol (ROH) with $H_3O^+\cdot(H_2O)_n$ (n = 0–3) as well as the secondary reactions of the H_3O^+/ROH product ions with H_2O (hydration) and ROH in view of their accurate quantification in ambient air samples with medium-pressure chemical ionization mass spectrometry (CIMS) instrumentation using H_3O^+ reactant ions.

Whereas water elimination following proton transfer was found to be the main mechanism for all H_3O^+/ROH reactions studied and for the $H_3O^+\cdot H_2O$/*trans*-2-hexen-1-ol reaction, all other $H_3O^+\cdot(H_2O)_n$/ROH (n = 1, 2) reactions proceeded by multiple reaction mechanisms. $H_3O^+\cdot(H_2O)_3$ reactions proceeded mainly (C_6 alcohols) or exclusively (C_5 alcohols) by ligand switching followed by water elimination. Hydration of the H_3O^+/ROH product ions was observed whenever they contained oxygen. The secondary reactions with ROH were also found to proceed by multiple reaction pathways.

1. Introduction

Biogenic non-methane volatile organic compounds (BVOCs) are known to be emitted in huge amounts (about 1150 Tg C yr^{-1} worldwide [1]) by terrestrial vegetation. An important fraction of these BVOCs consists of unsaturated compounds, which are highly reactive with the main atmospheric oxidants (O_3, $^\bullet OH$, $NO_3^\bullet$). In the presence of nitrogen oxides, their oxidation can lead to net oxidant formation, as well as to secondary organic aerosols (SOA).

In recent years, we have systematically studied the reactions of a number of BVOCs, e.g., monoterpenes [2], sesquiterpenes [3] and oxygenated species [4,5] with H_3O^+, NO^+ and $O_2^{+\bullet}$ ions in a laboratory selected ion flow tube (SIFT) apparatus and, in the case of sesquiterpenes, with $H_3O^+\cdot(H_2O)_n$ ions in a commercially available proton transfer reaction mass spectrometer (PTR-MS, Ionicon Analytik GmbH) [6]. These laboratory studies were carried out in support of the detection of these BVOCs by medium-pressure chemical ionization mass spectrometry (CIMS) flow and drift tube techniques.

In the course of the last decade, these techniques have continuously gained importance as analytical tools for the fast and sensitive on-line detection of many trace gases, with applications in very diverse fields such as atmospheric chemistry, breath analysis and food technology, amongst other. They are based on selective reactions between specific source ions, which do not react with the main atmospheric constituents, and the trace species of interest which result in specific product ions that are fingerprints of the species to be detected. In many applications, the ion chemistry in the reactor and therefore, also the detection and quantification of the trace gases is complicated by the presence of water vapour in the reactor. This problem is of great importance to CIMS techniques, which use H_3O^+ as reactant ion species, such as the thermal SIFT-MS technique and the PTR-MS technique. The development

* Corresponding author. Tel.: +32 2 373 03 90; fax: +32 2 373 84 23.
E-mail address: crist.amelynck@aeronomie.be (C. Amelynck).

1387-3806/$ – see front matter © 2009 Elsevier B.V. All rights reserved.
doi:10.1016/j.ijms.2009.04.001

of both techniques started in the mid-nineties and they have been continuously improved since then.

In the SIFT-MS technique, originally developed by Smith and Španěl [7], H_3O^+, NO^+ and $O_2^{+\bullet}$ reactant ions are simultaneously produced in a microwave discharge in a H_2O/air mixture and alternately injected in a flow tube reactor after being pre-selected in a quadrupole mass filter. Differences in ion chemistry associated with the different precursor ions can sometimes lead to selective detection of isobaric or even isomeric compounds. Details of the SIFT-MS technique can be found in many extensive review papers, e.g. Ref. [8]. Whereas NO^+ and $O_2^{+\bullet}$ ions have no large propensity for hydration, reactant H_3O^+ ions rapidly form higher order proton hydrates $H_3O^+\cdot(H_2O)_n$ (n = 1–3) by reaction with water vapour molecules, especially when trace gas analysis is performed in moist samples. For accurate quantification of a trace compound with the SIFT-MS technique using H_3O^+ reactant ions, the ion/molecule chemistry of the other proton hydrates with this compound has to be taken into account as well.

In the analytical PTR-MS technique, developed by Lindinger et al. [9] at the University of Innsbruck, Austria, H_3O^+ ions are produced in a hollow cathode discharge ion source and injected in a drift tube reactor in which they react with the trace gases contained in the sampled air. More details on the PTR-MS technique and its applications can be found in a recent extensive review by de Gouw and Warneke [10] and references therein. In a PTR-MS instrument, excessive hydration of reactant H_3O^+ ions is prevented at sufficiently high values of E/N in the drift tube reactor (E is the applied electric field and N is the buffer gas number density). In some cases, however, reduction of E/N can lead to enhanced sensitivity for the detection of specific compounds [6]. Modulation of E/N, and therefore of the proton hydrate distribution in the reactor, can even result in selective detection of isobaric compounds, as was recently demonstrated for 1-butene and acrolein [11]. For these and other applications, the ion chemistry of higher order proton hydrates with these compounds is surely worthy of investigation.

Over the years, SIFT instruments have proven to be very successful in providing kinetic and mechanistic information on gas phase ion/molecule reactions [12] and they are certainly useful to study the individual reactions taking place in CIMS flow tube reactors in the presence of water vapour. While using a microwave discharge ion source in an air/water vapour mixture, however, we were not able to inject hydrated hydronium ions into our SIFT reactor. Therefore we replaced this ion source by a flowing afterglow (FA) reactor. Apart from the possibility of introducing cluster ions, a tandem FA/SIFT instrument in principle allows introduction of all ion species, either positive or negative, that can be produced in the FA reactor through electron/neutral or ion/neutral interactions and that can be injected in the SIFT reactor without being lost by collision-induced dissociation (CID) in the SIFT injector. This FA/SIFT combination was already explored in the early eighties [13,14], but a big step forward in FA/SIFT instrumentation was taken when Van Doren et al. [15] at the University of Boulder, Colorado, succeeded in building a flowing afterglow selected ion flow drift tube (FA/SIFDT) with high ion transmission, mainly due to efficient pumping of the vacuum chamber behind the FA inlet orifice.

In the present paper, we will describe our newly built FA/SIFT instrument and some of its performance characteristics. The instrument has been validated by the study of the reactions of $H_3O^+\cdot(H_2O)_n$ ions with methanol and ethanol, as well as of some secondary reactions involved in this ion chemistry.

Subsequently, the validated instrument has been used for the ion/molecule reaction studies of $H_3O^+\cdot(H_2O)_n$ ions with four unsaturated alcohols, more particularly two pentenol isomers (2-methyl-3-buten-2-ol and 1-penten-3-ol) and two hexenol isomers (*cis*-3-hexen-1-ol and *trans*-2-hexen-1-ol), which are known to be emitted by terrestrial vegetation, either directly or after leaf wounding [16,17]. Hydration of the main product ions has also been studied, as well as some other secondary reactions which may take place when large amounts of these substances are admitted to the CIMS reactor. The results of these laboratory studies and possible implications for the detection of unsaturated alcohols using medium-pressure CIMS flow and drift tube techniques will be discussed.

2. Experimental

2.1. Instrument description

The newly developed FA-SIFT instrument, shown in Fig. 1, is an extension of our existing SIFT instrument, which was initially equipped with a low-pressure (0.21 hPa) microwave discharge ion source for the production of H_3O^+, NO^+ and $O_2^{+\bullet}$ reactant ions from a mixture of air and water vapour.

The new instrument consists of four sections: a flowing afterglow ion reactor, in which all kinds of reactant ions can be

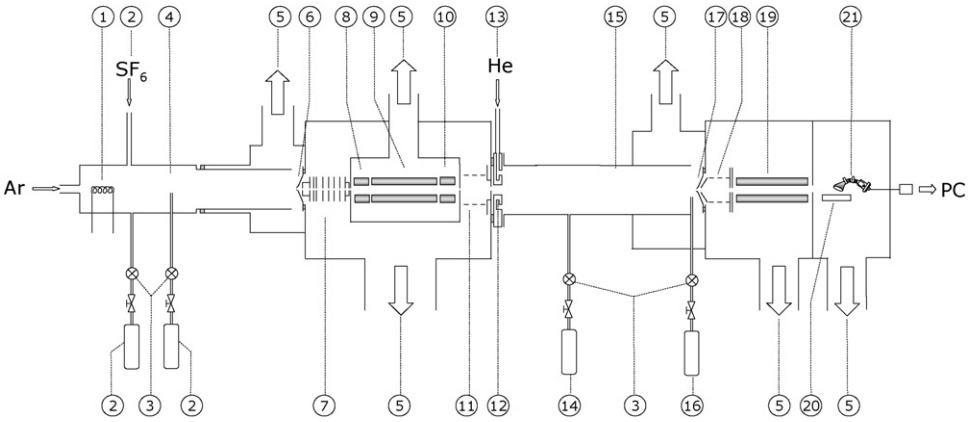

Fig. 1. Schematic representation of the FA-SIFT instrument: (1) Electron emitting filament, (2) reactant gas inlets, (3) needle valves, (4) FA flow tube, (5) to pumping system, (6) selection quadrupole chamber inlet flange, (7) lens system, (8) quadrupole pre-filter, (9) selection quadrupole, (10) quadrupole post-filter, (11) lens system, (12) Venturi injector, (13) He buffer gas inlet, (14) reactant inlet for kinetic measurements, (15) flow tube reactor, (16) reactant gas inlet for product ion distribution measurements, (17) mass spectrometer inlet flange, (18) lens system, (19) analyzing quadrupole, (20) conversion dynode, (21) electron multiplier.

produced through selective ion/molecule reactions, a reactant ion selection region, a flow tube reactor to study the kinetics and product ion distributions of the selected reactant ions with the neutral reactant of interest and finally, an ion detection section.

The FA section consists of a 70 cm long stainless steel tube in which a 30 STP $cm^3\,s^{-1}$ Ar flow is maintained by means of a large Roots pump (Edwards), resulting in a FA pressure of 0.44 hPa. Ar atoms are ionized by impact of electrons emitted by an emission current regulated thoria coated iridium filament, located 51 cm upstream of the flow tube end. To efficiently optimize the overall ion transmission of the instrument, the flow tube was designed in such a way that it can be polarized with respect to the instrument housing. This required a flow tube inner diameter reduction from 3.5 to 2.5 cm at a distance of 30 cm downstream of the filament. While being convected downstream the FA reactor by the buffer gas flow, the primary Ar^+ ions are converted to the SIFT reactant ions of interest by adding appropriate amounts of suitable neutral reactants to the afterglow. For this purpose, the FA reactor is equipped with three finger-shaped reactant gas inlets of which two are located opposite to each other at 8 cm and the third one at 20.5 cm downstream of the filament. In order to enhance the production of positive reactant ions, one of the inlets close to the filament is used to introduce a low flow of a 1000 ppm SF_6/Ar mixture to the afterglow, which results in attachment of free electrons to SF_6. This converts the positive ion/electron plasma into a positive ion/negative ion plasma resulting in slower ambipolar diffusion of positive ions to the stainless steel walls of the flow tube reactor and less ion loss due to recombination effects.

At the downstream end of the flow tube reactor, the ions are sampled into a high vacuum chamber through a 600 μm diameter inlet orifice in a biased conically shaped inlet flange (#6 in Fig. 1). In this vacuum chamber, which is pumped by a 1600 L s^{-1} turbomolecular pump (Pfeiffer Vacuum), the ions are subsequently guided by a set of electrostatic lenses to a selection quadrupole mass filter, equipped with a pre- and post-filter for optimal ion transmission, in which the reactant ions of interest are selected according to their m/z ratio. This mass filter is housed in a separate aluminum box inside the large vacuum chamber and pumped differentially with a 500 L s^{-1} turbomolecular pump (Pfeiffer Vacuum). By means of a second lens array, the mass-selected ions are transported towards the SIFT injector. The dimension of the inlet orifice between the FA reactor and the vacuum chamber and the pressure in the FA reactor are a trade-off between diffusional ion loss in the flow tube, ion transmission through the orifice and the pressure in the vacuum chamber which houses the electrostatic lens systems. The abovementioned values for the FA pressure and the orifice diameter are the outcome of an optimization process and result in pressures of 1.3×10^{-4} and 4.3×10^{-6} hPa and a corresponding Ar mean free path of 0.7 and 22 m in the lens system and differentially pumped quadrupole zone, respectively. Consequently, decrease in ion transmission efficiency due to collisions with Ar buffer gas atoms is negligible in these regions.

Pre-selected reactant ions enter the reaction region through the 0.75 mm central orifice of a biased SIFT Venturi injector (Birmingham design [18], #12 in Fig. 1) and are convectively transported downstream a second flow tube by a 100 STP $cm^3\,s^{-1}$ He carrier gas flow, introduced through a circular array of 12 holes with a diameter of 0.70 mm in the injector and maintained by a second Roots pump (Leybold). This results in a typical flow tube pressure of 1.4 hPa. The Venturi injector reduces He backstreaming into the ion selection region, resulting in a better vacuum in this region and less risk of decomposition of the reactant ions by collision-induced dissociation near the Venturi injector orifice. The reaction flow tube is made of stainless steel and has an inner diameter of 4 cm, a total length of 51 cm from injector to mass spectrometer inlet plate and is equipped with two reactant gas inlets. The first inlet, situated at 27 cm from the inlet plate, is used for kinetic measurements and the second one is used for product ion distribution measurements and is located at 0.8 cm from the inlet plate. At the downstream end of the flow tube, the source and product ions are sampled into a vacuum chamber through a 400 μm orifice in a conically shaped electrically biased inlet flange (#17 in Fig. 1). In this chamber, which is pumped by a set of three 300 L s^{-1} turbomolecular pumps (Varian), the ions are guided by a set of electrostatic lenses towards the detection quadrupole mass filter, in which they are analyzed according to their m/z ratio. Ions that are transmitted by the mass filter are detected by a differentially pumped secondary electron multiplier (DeTech), equipped with a conversion dynode and operated in pulse counting mode.

2.2. Production of SIFT reactant ions in the FA reactor and their injection into the SIFT reactor

The SIFT reactant ions of interest in this paper are the proton hydrates $H_3O^+\cdot(H_2O)_n$ (n = 0–3) and the reaction products of H_3O^+ ions with unsaturated biogenic alcohols. All ions were produced starting from Ar^+ ions, which in turn were produced by electron impact ionization as described in the previous paragraph. In the Ar buffer gas flow, part of the Ar^+ ions are converted into molecular Ar_2^+ ions by three-body association. By adding controlled amounts of H_2O vapour downstream of the filament ion source, a series of ion/molecule reactions takes place, resulting in the formation of H_3O^+. When introducing even larger quantities of water vapour, hydrated H_3O^+ clusters can be created. Reaction products of the unsaturated biogenic alcohols with H_3O^+ can be created by introduction of the corresponding neutral further downstream the FA reactor.

Upon injection in the reactor zone, these reactant ions may undergo collision-induced dissociation in the vicinity of the injection orifice by collisions with the backstreaming helium gas. The kinetic energy of these ions near the injector orifice is determined by the potential difference between the FA inlet plate and the SIFT injector plate. In order to extract the positive ions into the flow tube, which is at ground potential, it is necessary to put a positive potential on the SIFT injector plate. The potential on the FA inlet plate and on the FA reactor itself need to be adapted accordingly.

The absolute count rates and relative contributions of source/fragment ions for $H_3O^+\cdot(H_2O)_n$ (n = 1–3) versus the center of mass energy (E_{cm}) of the corresponding source ion, are given in Fig. 2. The choice of the optimum value of E_{cm} depends on two criteria: a sufficiently high reactant ion signal (>1000 cps) and only a minor contribution of impurities to the spectrum (<10%). Injection of $H_3O^+\cdot H_2O$ (Fig. 2a) at 1.0 eV resulted in only a minor contribution of H_3O^+ (0.7%) and an acceptable $H_3O^+\cdot H_2O$ count rate. Because of CID, $H_3O^+\cdot(H_2O)_2$ ions could not be introduced in the SIFT reactor in a clean way by injection of a pre-selected $H_3O^+\cdot(H_2O)_2$ ion beam (Fig. 2b). However, when a pre-selected $H_3O^+\cdot(H_2O)_3$ beam was injected at 0.7 eV, large amounts of $H_3O^+\cdot(H_2O)_2$ were created by CID with no interferences from $H_3O^+\cdot(H_2O)_3$ and only minor interference from $H_3O^+\cdot H_2O$ (Fig. 2c). The optimal condition to introduce $H_3O^+\cdot(H_2O)_3$ ions in the SIFT was obtained by injecting pre-selected $H_3O^+\cdot(H_2O)_3$ at an E_{cm} value of 0.5 eV. During injection, however, 80% of these ions still lose a water ligand by CID.

To ascertain that the $H_3O^+\cdot(H_2O)_2$ ions in the flow tube were due to CID of the parent $H_3O^+\cdot(H_2O)_3$ ions upon injection in the flow tube and not to thermal decomposition of the latter ion species

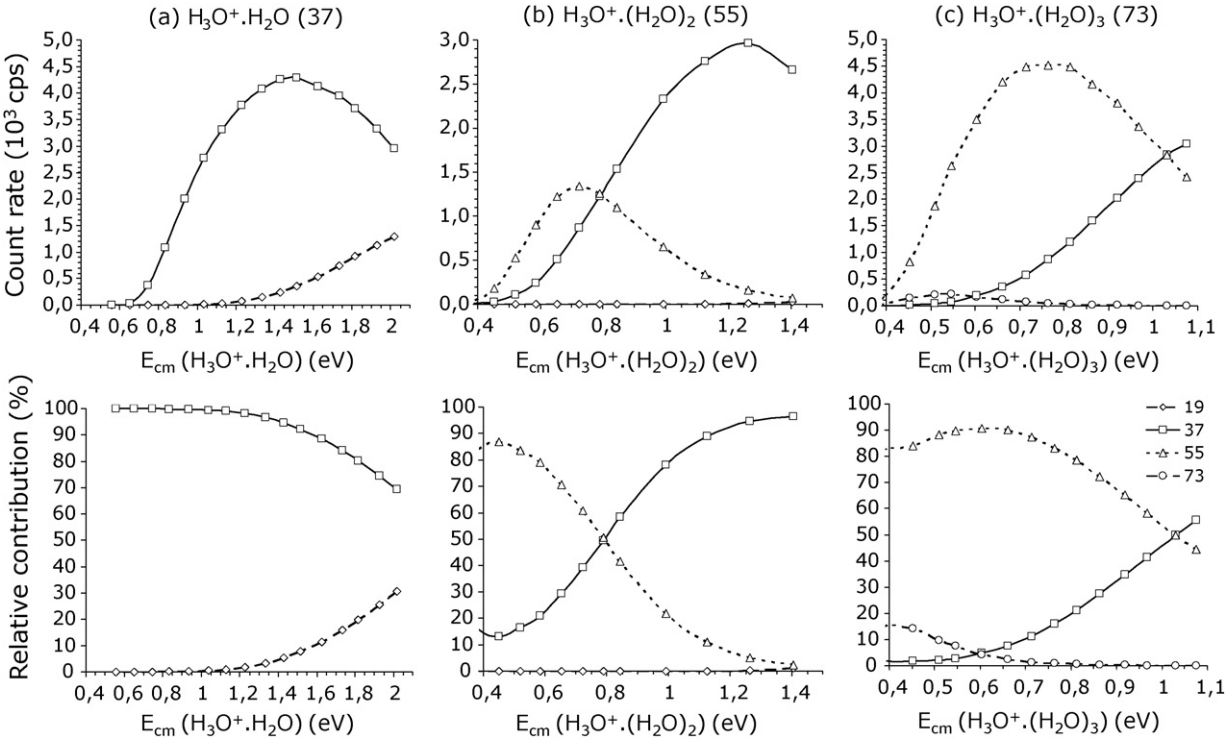

Fig. 2. Count rate and relative contribution of proton hydrates when injecting $H_3O^+{\cdot}H_2O$ (a), $H_3O^+{\cdot}(H_2O)_2$ (b) and $H_3O^+{\cdot}(H_2O)_3$ (c) as function of the center of mass energy of the injected ion.

in the flow tube, an estimation was made of the $H_3O^+{\cdot}(H_2O)_3$ lifetime for thermal dissociation at room temperature (298 K). This estimation is based on literature data by Lau et al. [19] and takes into account that the efficiency of collisional stabilization of the nascent excited ion/water complex by He is on average 0.23 times lower than by CH_4 as a third body [20]. The resulting lifetime is ~500 ms and the ion residence time in the flow tube is 5.2 ms, resulting in minor ion loss by thermal decomposition (~1%).

2.3. Measuring methods

Reproducible reaction rate constants have been obtained by introducing volumetric mixtures of the reactant neutrals prepared in volume calibrated glass bottles in He into the flow tube through a heated needle valve. The temperature of the needle valve and the tubing was kept at 40 °C for all compounds, except for the temperature-sensitive *trans*-2-hexen-1-ol, for which, as a precaution, the tubing was not heated. The reactant gas flow was determined by monitoring the pressure decay in the glass bottles as a function of time and for each reaction at least three different mixing ratios were used. The rate constants have been obtained from the logarithmic decay of the reactant ion signal as a function of the compound concentration in the flow tube. The reaction time has been determined experimentally and was found to be 2.8 ms at typical conditions of flow rate and pressure in the SIFT reactor.

Product ion distributions (PIDs) were determined by operating the mass spectrometer in the multi-ion-mode (MIM) and by introducing the compounds at the inlet close to the mass spectrometer inlet orifice to minimize distortion by diffusion enhancement effects and possible secondary reactions.

As already mentioned in Section 2.2, even at the optimal conditions for introduction of $H_3O^+{\cdot}(H_2O)_3$ in the SIFT reactor, 80% of the reactant ions is still made up of $H_3O^+{\cdot}(H_2O)_2$ ions. Consequently, in order to obtain PIDs of $H_3O^+{\cdot}(H_2O)_3$ reactions, product ion signals originating from this mixture of reactant ions have been corrected for the contribution of product ions of $H_3O^+{\cdot}(H_2O)_2$ reactions by taking into account accurate PIDs of $H_3O^+{\cdot}(H_2O)_2$ reactions and the $[H_3O^+{\cdot}(H_2O)_3]/[H_3O^+{\cdot}(H_2O)_2]$ ratio in the SIFT reactor. Similarly PIDs of $H_3O^+{\cdot}(H_2O)_2$ reactions have been corrected for the minor contribution of interfering $H_3O^+{\cdot}H_2O$ ions in the reactor.

Also, accurate determination of PIDs requires that the mass discrimination of the mass spectrometer system is well-known.

In our previous SIFT experiments, an adequate correction for mass discrimination was obtained according to a method described by Španěl and Smith [21]. In this method, several specific volatile organic compounds were introduced alternately in the SIFT reactor. Addition of sufficient amounts of each of these gases leads to a single terminal ion species at the downstream end of the flow tube reactor, for instance MH^+ in the case of the aromatic species benzene, toluene and *m*-xylene and M_2H^+ for the ketones acetone, 2-butanone and 3-pentanone. The mass discrimination factor (MDF) for these ions was then obtained from the ratio of the count rate for the terminal ion species to the terminal ion current on the mass spectrometer inlet plate relative to this ratio obtained for H_3O^+ ions.

In the FA-SIFT apparatus, however, clean injection of typical product ion species originating from the ion/molecule reactions studied is possible, resulting in MDF values for these specific ions instead of approximative values as obtained by the previous technique. This results in a better mass discrimination correction for these specific ions. Mass discrimination over the entire useful mass range (MDF as a function of m/z) is obtained regularly by fitting a curve through these individual data points.

Table 1
Rate constants and product ion distributions for the methanol reactions. Values available from literature are obtained at a temperature close to 300 K. Numbers between square brackets indicate the reference number at the end of the article.

Reactant ion	Product ion distribution		Reaction rates constants (10^{-9} cm^3 molecule^{-1} s^{-1})		
	Product ions	(%)	k_{COL}	k_{EXP}	k_{LIT}
H_3O^+ (19)	$CH_3OH_2^+$ (33)	100	2.7	2.6	2.1[a,1], 2.2[a,2], 2.4[b], 2.7[c], 2.8[d], 3.8[e]
$H_3O^+\cdot H_2O$ (37)	$CH_3OH_2^+\cdot H_2O$ (51)	100	2.3	2.2	1.9[b], 2.0[a], 2.4[f]
$H_3O^+\cdot(H_2O)_2$ (55)	$CH_3OH_2^+\cdot(H_2O)_2$ (69)	100	2.1	2.0	1.9[b], 2.0[f]
$H_3O^+\cdot(H_2O)_3$ (73)	$CH_3OH_2^+\cdot(H_2O)_3$ (87)	100	2.0	1.9	<0.01[b], 1.9[f]
$CH_3OH_2^+$ (33)	$(CH_3)_2OH^+$ (47)	15	2.3	0.70	0.076[g,1], 0.09[h], 0.104[i], 0.105[j], 0.108[k], 0.46[l], 0.51[g,2]
	$(CH_3OH)_2H^+$ (65)	83			
	Others	2			
$CH_3OH_2^+\cdot H_2O$ (51)	$(CH_3OH)_2H^+$ (65)	100	2.1	2.2	N/A
$(CH_3OH)_2H^+$ (65)	$(CH_3)_2OH^+\cdot CH_3OH$ (79)	4	2.0	0.34	0.24[g,3]
	$(CH_3OH)_3H^+$ (97)	95			
	Others	1			

[a,1][25], FA; [a,2][25], FDT; [b][26], SIFT, 0.67 hPa; [c][27], SIFT, 0.67 hPa; [d][28], FA, 0.34–0.68 hPa; [e][29], FA, 1.7 hPa; [f][30], FA, 0.34–0.68 hPa; [g,1][31], SIFT, 0.73 hPa, $(CH_3)_2OH^+$ channel; [g,2][31], SIFT, 0.73 hPa, $(CH_3)_2OH^+ + (CH_3OH)_2H^+$ channel; [g,3][31], SIFT, 0.76 hPa; [h][32], ICR, 1.3×10^{-3} to 1.3×10^{-6} hPa; [i][33], FTICR, 1×10^{-8} to 9×10^{-8} hPa; [j][34], ICR, 1.3×10^{-5} hPa; [k][35], ICR, 1.3×10^{-5} to 1.3×10^{-6} hPa; [l][36], FA-SIFT, 0.63 hPa.

2.4. Chemicals used

2-Methyl-3-buten-2-ol (98%, Aldrich), *cis*-3-hexen-1-ol (98%, Aldrich), *trans*-2-hexen-1-ol (96%, Aldrich), 1-penten-3-ol (99%, Acros), methanol (99.8%, Merck) and ethanol (99.9%, Fluka) were obtained commercially as indicated. Ar and He buffer gases are obtained from Air Products and are of BIP grade (99.9997%). The 1000 ppm SF_6/Ar mixture has been bought from Air Products.

3. Results and discussion

In a first part of this paragraph, the validation of our newly built FA-SIFT instrument, involving ion/molecule reactions with methanol and ethanol, will be discussed. Subsequently, the reactions of $H_3O^+\cdot(H_2O)_n$ ions (n = 0–2) with four biogenic alcohols will be addressed and finally, secondary reactions associated with ions produced in the H_3O^+/alcohol reactions will be reported.

The purity of the individual reactant ions in the SIFT reactor is at least 90% and product ion distributions have been corrected for the presence of product ions related to the presence of impurity reactant ions when possible. Only product ions with a branching ratio of 2% or higher are mentioned in the product ion distribution tables. The remaining minor product ions are gathered together as "other".

The accuracy of the branching ratios of the reactions involving $H_3O^+\cdot(H_2O)_{0-2}$ is at most 12% and decreases to 5% for branching ratios above 25%. Because of the coexistence of $H_3O^+\cdot(H_2O)_2$ and $H_3O^+\cdot(H_2O)_3$ in the experiments that were performed to study the ion chemistry of $H_3O^+\cdot(H_2O)_3$ ions, and the fact that some of the observed product ions originated from both reactant ions, the accuracy of branching ratios for reactions with $H_3O^+\cdot(H_2O)_3$ ions was as high as 25% for the most abundant channels and increases to as much as 50% for less abundant channels which have product ions in common with the $H_3O^+\cdot(H_2O)_2$ reactions.

The precision of the experimentally determined rate constants (k_{EXP}) is ~8%, while the results are accurate within 25%. The measured rate constants are compared with literature data (k_{LIT}) when available and with calculated collision rate constants (k_{COL}). The latter were obtained with the parameterized theory of Su and Chesnavich [22,23]. For these calculations, values of 3.29 and 5.84 Å^3 for the polarizability and 1.70 and 1.69 D for the electric dipole moment of methanol and ethanol, respectively, were taken into account [24]. Values for the polarizabilities and electric dipole moments of the C_5 and C_6 alcohols were obtained from quantum chemical calculations [5].

3.1. Instrument validation

The FA-SIFT has been validated by measuring rate constants and product ion distributions of the well-documented reactions of methanol and ethanol with $H_3O^+\cdot(H_2O)_n$ (n = 0–2) ions and with their corresponding proton transfer product MH^+. In addition the reactions of these two alcohols with their corresponding cluster ions $MH^+\cdot H_2O$ and M_2H^+ have been studied and rate constant measurements of the protonated alcohols with H_2O vapour have been performed as well.

3.1.1. Methanol reactions

As shown in Table 1, the reactions of methanol with the hydrated hydronium ions $H_3O^+\cdot(H_2O)_n$ (n = 0–2) are all found to proceed at the collision rate, which is in agreement with previously reported literature data [25–30]. The $H_3O^+\cdot(H_2O)_3$/methanol reaction has been investigated in the past by Böhme et al. [30] and by Španěl and Smith [26]. Whereas the latter authors reported that this reaction did not take place, the former found the reaction to occur at the collision rate, which is in agreement with our results.

The reaction of H_3O^+ ions solely results in the protonated methanol ion, whereas the reactions with $H_3O^+\cdot H_2O$, $H_3O^+\cdot(H_2O)_2$ and $H_3O^+\cdot(H_2O)_3$ ions entirely proceed by ligand switching (reactions (1)–(4)).

$$H_3O^+ + CH_3OH \rightarrow CH_3OH_2^+ + H_2O, \quad \Delta_r G^\circ = -65\ \text{kJ mol}^{-1} \tag{1}$$

$$H_3O^+\cdot H_2O + CH_3OH \rightarrow CH_3OH_2^+\cdot H_2O + H_2O, \quad \Delta_r G^\circ = -42\ \text{kJ mol}^{-1} \tag{2}$$

$$H_3O^+\cdot(H_2O)_2 + CH_3OH \rightarrow CH_3OH_2^+\cdot(H_2O)_2 + H_2O, \quad \Delta_r G^\circ = -38\ \text{kJ mol}^{-1} \tag{3}$$

$$H_3O^+\cdot(H_2O)_3 + CH_3OH \rightarrow CH_3OH_2^+\cdot(H_2O)_3 + H_2O, \quad \Delta_r G^\circ = -30\ \text{kJ mol}^{-1} \tag{4}$$

Standard reaction free energies of reactions (1)–(4) were calculated using thermodynamic values from the literature [37,38].

For the $H_3O^+\cdot(H_2O)_2$/methanol reaction, an additional $CH_3OH_2^+\cdot H_2O$ product ion with a yield of 40% has been reported

Table 2
Rate constants and product ion distributions for the ethanol reactions. Values available from literature are obtained at a temperature close to 300 K. Numbers between square brackets indicate the reference number at the end of the article.

Reactant ion	Product ion distribution		Reaction rates constants (10^{-9} cm^3 molecule^{-1} s^{-1})		
	Product ions	(%)	k_{COL}	k_{EXP}	k_{LIT}
H_3O^+ (19)	$C_2H_5OH_2^+$ (47)	100	2.7	2.6	2.7[a,b], 2.8[c], 3.8[d]
$H_3O^+\cdot H_2O$ (37)	$C_2H_5OH_2^+\cdot H_2O$ (65)	100	2.2	2.3	2.3[a], 2.5[e]
$H_3O^+\cdot(H_2O)_2$ (55)	$C_2H_5OH_2^+\cdot H_2O$ (65) $C_2H_5OH_2^+\cdot(H_2O)_2$ (83)	10 90	2.0	2.1	2.1[a], 2.0[e]
$H_3O^+\cdot(H_2O)_3$ (73)	$C_2H_5OH_2^+\cdot H_2O$ (65) $C_2H_5OH_2^+\cdot(H_2O)_2$ (83) $C_2H_5OH_2^+\cdot(H_2O)_3$ (101)	20 16 64	1.9	1.8	<0.01[b], 1.7[e]
$C_2H_5OH_2^+$ (47)	$(C_2H_5OH)_2H^+$ (93)	100	2.1	1.7	0.068[f], 0.074[g], 2.2[h], 2.4[h]
$C_2H_5OH_2^+\cdot H_2O$ (65)	$(C_2H_5OH)_2H^+$ (93)	100	1.9	2.0	N/A
$(C_2H_5OH)_2H^+$ (93)	$(C_2H_5OH)_3H^+$ (139)	100	1.8	0.78	N/A

[a][26], SIFT, 300 K, 0.67 hPa; [b][27], SIFT, 300 K, 0.67 hPa; [c][28], FA, 298 K, 0.34–0.68 hPa; [d][29], FA, 300 K, 1.7 hPa; [e][30], FA, 0.34–0.68 hPa: [f][35], ICR, 320 K, 1.3×10^{-5} to 1.3×10^{-6} hPa; [g][40], FTICR, 5.9×10^{-9} to 1.3×10^{-8} hPa; [h][34], ICR, 1.3×10^{-5} hPa.

for the SIFT study by Španěl and Smith [26]. However, we did not observe this product ion, which is consistent with thermodynamics since the reaction free energy of this reaction pathway is calculated to be +14 kJ mol^{-1}.

The reaction of protonated methanol with methanol has been investigated on several occasions using different techniques as shown in Table 1. A highly detailed FA-SIFT study of this reaction was performed by Dang and Bierbaum [36]. According to these authors, the reaction proceeds by proton transfer (5a), condensation (5b) and termolecular association (5c):

$$CH_3OH_2^+ + \underline{C}H_3OH \rightarrow \underline{C}H_3OH_2^+ + CH_3OH \quad (5a)$$

$$CH_3OH_2^+ + CH_3OH \rightarrow (CH_3)_2OH^+ + H_2O \quad (5b)$$

$$CH_3OH_2^+ + CH_3OH \xrightarrow{M} (CH_3OH)_2H^+ \quad (5c)$$

They were able to quantify the hidden proton transfer channel through isotopic labeling of the reactants with ^{18}O and deuterium and, by taking into account this hidden channel, they found the overall reaction to proceed at the collision rate.

In our experiments, yields of 15% and 83% were observed for the condensation product ion and the association product ion, respectively. When correcting these product ion distributions for the presence of a hidden proton transfer channel by assuming that the overall reaction takes place at the collision rate, branching ratios of 70% for the proton transfer channel, 5% for the condensation channel and 25% for the association channel are obtained. Dang and Bierbaum reported values of 85%, 4% and 11% for the respective reaction channels. The lower contribution of the association product they obtained may be explained by the lower operating pressure in their SIFT reactor (only 0.63 hPa, in contrast to 1.43 hPa in our experiments). Furthermore, our value for the branching ratio of the condensation channel is close to theirs, which is in agreement with the generally observed pressure independence of this reaction pathway. When taking into account the branching ratio for the pressure independent condensation channel, reaction rate constants of 0.09–0.11 $\times 10^{-9}$ cm^3 molecule^{-1} s^{-1} can be found for low-pressure techniques such as ion cyclotron resonance (ICR), which is in good agreement with literature values.

Finally, the reactions of hydrated protonated methanol and of the proton-bound methanol dimer with methanol have been studied. The former reaction proceeds by ligand switching (reaction (6)) and is found to occur at the collision rate.

$$CH_3OH_2^+\cdot H_2O + CH_3OH \rightarrow (CH_3OH)_2H^+ + H_2O \quad (6)$$

The $(CH_3OH)_2H^+$/methanol reaction mainly proceeds by three-body association (reaction (7a)) similar to the $CH_3OH_2^+$/methanol reaction, but in contrast to Morris et al. [31], a minor condensation product ion (reaction (7b)) has been observed. The comparison of the experimental termolecular reaction rate constant for this reaction (9.6×10^{-27} cm^6 s^{-1}) to the literature value of 1.3×10^{-26} cm^6 s^{-1} indicates that at the SIFT operation pressure, the fall-off region of the apparent second-order rate constant is reached.

$$(CH_3OH)_2H^+ + CH_3OH \xrightarrow{M} (CH_3OH)_3H^+ \quad (7a)$$

$$(CH_3OH)_2H^+ + CH_3OH \rightarrow (CH_3)_2OH^+\cdot CH_3OH + H_2O \quad (7b)$$

3.1.2. Ethanol reactions

The reactions of ethanol with $H_3O^+\cdot(H_2O)_n$ (n = 0–3) are also found to proceed at the collision rate, as can be noticed in Table 2. This is in agreement with previously reported literature data for n = 0–2 and the literature data of Böhme et al. [30] for n = 3. Similar as in the case of methanol, our data on the $H_3O^+\cdot(H_2O)_3$/ethanol reaction are in disagreement with the observations of Španěl and Smith [26], who reported that this reaction did not take place in their SIFT instrument.

The reaction of H_3O^+ results exclusively in the protonated ethanol ion, whereas the reaction with $H_3O^+\cdot H_2O$ proceeds only by ligand switching. The main reaction mechanism of the $H_3O^+\cdot(H_2O)_2$/ethanol reaction is ligand switching, but a small contribution of the $C_2H_5OH_2^+\cdot H_2O$ product ion, has also been observed. For the $H_3O^+\cdot(H_2O)_3$/ethanol reaction the ligand switching product has been found, but also $C_2H_5OH_2^+\cdot(H_2O)_2$ and $C_2H_5OH_2^+\cdot H_2O$ fragments were detected (see reactions (11a)–(11c)).

$$H_3O^+ + C_2H_5OH \rightarrow C_2H_5OH_2^+ + H_2O,$$
$$\Delta_r G^\circ = -87\ \text{kJ mol}^{-1} \quad (8)$$

$$H_3O^+\cdot H_2O + C_2H_5OH \rightarrow C_2H_5OH_2^+\cdot H_2O + H_2O,$$
$$\Delta_r G^\circ = -56\ \text{kJ mol}^{-1} \quad (9)$$

$$H_3O^+\cdot(H_2O)_2 + C_2H_5OH \rightarrow C_2H_5OH_2^+\cdot(H_2O)_2 + H_2O,$$
$$\Delta_r G^\circ = -45\ \text{kJ mol}^{-1} \quad (10a)$$

$$H_3O^+\cdot(H_2O)_2 + C_2H_5OH \rightarrow C_2H_5OH_2^+\cdot H_2O + 2H_2O,$$
$$\Delta_r G^\circ = +0.2\ \text{kJ mol}^{-1} \quad (10b)$$

$$H_3O^+\cdot(H_2O)_3 + C_2H_5OH \rightarrow C_2H_5OH_2{}^+\cdot(H_2O)_3 + H_2O, \quad \Delta_r G^\circ = -35\,kJ\,mol^{-1} \quad (11a)$$

$$H_3O^+\cdot(H_2O)_3 + C_2H_5OH \rightarrow C_2H_5OH_2{}^+\cdot(H_2O)_2 + 2H_2O, \quad \Delta_r G^\circ = -8\,kJ\,mol^{-1} \quad (11b)$$

$$H_3O^+\cdot(H_2O)_3 + C_2H_5OH \rightarrow C_2H_5OH_2{}^+\cdot H_2O + 3H_2O, \quad \Delta_r G^\circ = +37\,kJ\,mol^{-1} \quad (11c)$$

Standard reaction free energies of reactions (8)–(11) were again calculated using thermodynamic values from the literature [38,39].

The experimental results are in good agreement with literature data, except for the $H_3O^+\cdot(H_2O)_2$ reaction for which Smith and Španěl reported a 30% contribution of reaction (10b) [26], which is three times higher than the value that was obtained in the present study. Taking into account the errors on the thermodynamic values needed for the calculation of $\Delta_r G^\circ$ for reaction (10b), the observation of the $C_2H_5OH_2{}^+\cdot H_2O$ product ion is not in conflict with thermodynamic considerations. According to the calculated standard reaction free energy for the $H_3O^+\cdot(H_2O)_3/C_2H_5OH$ reaction, ligand switching followed by boil-off of two H_2O molecules should not occur. Nevertheless this pathway was found to have a 20% contribution. However, it should be noted that the uncertainty on the branching ratio of this pathway is large since the PID of the $H_3O^+\cdot(H_2O)_3/C_2H_5OH$ reaction was inferred from experiments in which $H_3O^+\cdot(H_2O)_2$ and $H_3O^+\cdot(H_2O)_3$ coexisted in the SIFT reactor, as explained in Section 2.2, and $C_2H_5OH_2{}^+\cdot H_2O$ was also found to be a product ion of the $H_3O^+\cdot(H_2O)_2/C_2H_5OH$ reaction.

Only the association product (reaction (12b)) was observed for the reaction of protonated ethanol ($C_2H_5OH_2{}^+$) with ethanol. Similar to the protonated methanol/methanol reaction, a hidden proton transfer channel (reaction (12a)) was observed through the presence of the isotope at m/z 48 when injecting $C_2H_5OH_2{}^+$ at m/z 47.

The reaction of hydrated protonated ethanol ($C_2H_5OH_2{}^+\cdot H_2O$) with ethanol proceeds at every collision by ligand switching (reaction (13)):

$$C_2H_5OH_2{}^+ + \underline{C}_2H_5OH \rightarrow \underline{C}_2H_5OH_2{}^+ + C_2H_5OH \quad (12a)$$

$$C_2H_5OH_2{}^+ + C_2H_5OH \xrightarrow{M} (C_2H_5OH)_2H^+ \quad (12b)$$

$$C_2H_5OH_2{}^+\cdot H_2O + C_2H_5OH \rightarrow (C_2H_5OH)_2H^+ + H_2O \quad (13)$$

The $(C_2H_5OH)_2H^+$/ethanol reaction proceeds by termolecular association (reaction (14)).

$$(C_2H_5OH)_2H^+ + C_2H_5OH \xrightarrow{M} (C_2H_5OH)_3H^+ \quad (14)$$

To our knowledge, the rate constants and product ion distributions of reactions (13) and (14) have not yet been reported in the literature.

3.1.3. Hydration of protonated methanol and protonated ethanol

Hydration of precursor and product ions in CIMS techniques is an important process which has to be taken into account for proper quantification of trace gases. In this respect the rate constants for termolecular association of hydronium ions, protonated methanol and protonated ethanol ions with water vapour have also been determined and are shown and evaluated against existing literature data in Table 3. Despite differences in the operating He pressure in the three SIFT instruments (varying between 0.3 and 2.0 hPa) involved in this data comparison, the third-order rate constants are in very close agreement, indicating that the fall-off region of the apparent second-order rate constants is not yet reached at these pressures.

Table 3
Termolecular association rate constants for the reactions of H_3O^+, $CH_3OH_2{}^+$ and $C_2H_5OH_2{}^+$ with H_2O.

Reactant ion	Reaction rate constants (10^{-27} cm^6 s^{-1})	
	k_{LIT}	k_{EXP}
H_3O^+	0.6 [41], 0.68 [42]	0.6
$CH_3OH_2{}^+$	2 [41]	2.1
$C_2H_5OH_2{}^+$	6 [41]	6.4

3.2. $H_3O^+\cdot(H_2O)_n$ reactions (n = 0,1,2) with unsaturated biogenic C_5 and C_6 alcohols

After having studied a set of ion/molecule reactions for validation purposes, the reactions of $H_3O^+\cdot(H_2O)_n$ ions with two C_5 (2-methyl-3-buten-2-ol and 1-penten-3-ol) and two C_6 alcohols (*cis*-3-hexen-1-ol and *trans*-2-hexen-1-ol) have been characterized.

The rate constants and an indication of the product ions for the reactions of H_3O^+ with 2-methyl-3-buten-2-ol, *cis*-3-hexen-1-ol and *trans*-2-hexen-1-ol have been reported previously in a FA-SIFT study by Custer et al. [43]. More recently, rate constants and product ions distributions for the H_3O^+ reactions with all four compounds were also obtained in our SIFT instrument in an ion/molecule reaction study of H_3O^+, NO^+ and $O_2{}^{+\bullet}$, the three common SIFT-MS precursor ions, with a series of biogenic C_5, C_6 and C_8 unsaturated alcohols [5]. For the sake of completeness and in order to verify whether the determination of mass discrimination is not affected by the method used, the reactions of H_3O^+ ions with the four compounds have been repeated in the present study.

Rate constant values for the reactions of $H_3O^+\cdot H_2O$ ions with the four compounds were also reported in our previous SIFT study, but they were obtained relative to the H_3O^+ rate constants by using a method described in Michel et al. [44]. In the present study, however, the possibility to cleanly introduce $H_3O^+\cdot H_2O$ enabled the absolute determination of these rate constants and, importantly, accurate product ion distributions of these reactions. As far as we know, no rate constants and product ion distributions have been reported yet for the reactions of $H_3O^+\cdot(H_2O)_2$ ions with C_5 and C_6 alcohols.

3.2.1. Reactions with 2-methyl-3-buten-2-ol and 1-penten-3-ol

As can be noticed in Table 4, the experimental rate constants of the $H_3O^+\cdot(H_2O)_n/C_5$ (n = 0–3) reactions obtained in the present study are in good agreement with the available literature values and are very close to the calculated collision rate constants.

The H_3O^+/2-methyl-3-buten-2-ol reaction is found to proceed for 80% via dissociative proton transfer, resulting in a $C_5H_9{}^+$ fragment due to elimination of a water molecule following proton transfer, and for 19% via non-dissociative proton transfer. The $C_6H_9{}^+$ (m/z 81) fragment ion, previously reported as a major product ion by Custer et al. [43], has not been observed. However, this ion has been detected when studying the secondary reaction of protonated 2-methyl-3-buten-2-ol with 2-methyl-3-buten-2-ol (see § 3.3.1), indicating that it is probably a secondary product ion of the H_3O^+/2-methyl-3-buten-2-ol reaction rather than a primary product ion.

The reaction of H_3O^+ with 1-penten-3-ol results for 90% in dissociative proton transfer, leading to the fragment ions $C_2H_5O^+$ (4%, reaction (15a)) and $C_5H_9{}^+$ (86%, reaction (15b)), and for 11% in non-dissociative proton transfer (reaction (15c)):

$$C_5H_9OH + H_3O^+ \rightarrow C_2H_5O^+ + \text{neutrals} \quad (15a)$$

$$C_5H_9OH + H_3O^+ \rightarrow C_5H_9{}^+ + 2H_2O \quad (15b)$$

Table 4
Rate constants and product ion distributions for the $H_3O^+\cdot(H_2O)_n/C_5$ reactions.

Neutral reactant	Reactant ion	Product ion distribution		Reaction rates constants (10^{-9} cm^3 molecule^{-1} s^{-1})		
		Product ions	(%)	k_{COL}	k_{EXP}	k_{LIT}
2-Methyl-3-buten-2-ol (86)	H_3O^+ (19)	$C_5H_9^+$ (69) $C_5H_9OH_2^+$ (87) Other	80 19 1	2.7	2.5	2.6[5], 2.2[43]
	$H_3O^+\cdot H_2O$ (37)	$C_5H_9^+$ (69) $C_5H_9OH_2^+$ (87) $C_5H_9OH_2^+\cdot H_2O$ (105)	50 46 4	2.1	2.1	2.3[5]
	$H_3O^+\cdot(H_2O)_2$ (55)	$C_5H_9OH_2^+\cdot H_2O$ (105) $C_5H_9OH_2^+\cdot(H_2O)_2$ (123) Other	61 38 1	1.8	1.9	N/A
	$H_3O^+\cdot(H_2O)_3$ (73)	$C_5H_9OH_2^+\cdot(H_2O)_2$ (123)	100	1.7	1.7	N/A
1-Penten-3-ol (86)	H_3O^+ (19)	$C_2H_5O^+$ (45) $C_5H_9^+$ (69) $C_5H_9OH_2^+$ (87)	4 86 10	2.7	2.6	2.6[5]
	$H_3O^+\cdot H_2O$ (37)	$C_5H_9^+$ (69) $C_5H_9OH_2^+$ (87) $C_5H_9OH_2^+\cdot H_2O$ (105) Other	72 18 9 1	2.1	2.2	2.0[5]
	$H_3O^+\cdot(H_2O)_2$ (55)	$C_5H_9OH_2^+\cdot H_2O$ (105) $C_5H_9OH_2^+\cdot(H_2O)_2$ (123)	48 52	1.8	1.9	N/A
	$H_3O^+\cdot(H_2O)_3$ (73)	$C_5H_9OH_2^+\cdot(H_2O)_2$ (123)	100	1.7	1.7	N/A

$$C_5H_9OH + H_3O^+ \rightarrow C_5H_9OH_2^+ + H_2O \quad (15c)$$

The PIDs and rate constants of the reactions of H_3O^+ with both 2-methyl-3-buten-2-ol and 1-penten-3-ol are in perfect agreement with the results obtained in our previous SIFT study of these compounds [5], which gives us confidence in the repeatability of experiments with the instrument.

$H_3O^+\cdot H_2O/C_5$ reactions mainly proceed via non-dissociative proton transfer (reaction (16b)) and water elimination following proton transfer (reaction (16a)), but also a small ligand switching channel (reaction (16c)) has been observed.

$$C_5H_9OH + H_3O^+\cdot H_2O \rightarrow C_5H_9^+ + 3H_2O \quad (16a)$$

$$C_5H_9OH + H_3O^+\cdot H_2O \rightarrow C_5H_9OH_2^+ + 2H_2O \quad (16b)$$

$$C_5H_9OH + H_3O^+\cdot H_2O \rightarrow C_5H_9OH_2^+\cdot H_2O + H_2O \quad (16c)$$

The reactions of $H_3O^+\cdot(H_2O)_2$ with the C_5 alcohols are found to proceed by ligand switching (reaction (17b)) and ligand switching followed by H_2O elimination (reaction (17a)). No proton transfer product was observed for these reactions.

$$C_5H_9OH + H_3O^+\cdot(H_2O)_2 \rightarrow C_5H_9OH_2^+\cdot H_2O + 2H_2O \quad (17a)$$

$$C_5H_9OH + H_3O^+\cdot(H_2O)_2 \rightarrow C_5H_9OH_2^+\cdot(H_2O)_2 + H_2O \quad (17b)$$

The reactions of $H_3O^+\cdot(H_2O)_3$ with both C_5 alcohols were found to proceed exclusively by ligand switching followed by H_2O elimi-

Table 5
Rate constants and product ion distributions for the $H_3O^+\cdot(H_2O)_n/C_6$ reactions.

Neutral reactant	Reactant ion	Product ion distribution		Reaction rates constants		
		(10^{-9} cm^3 molecule^{-1} s^{-1})	(%)	k_{COL}	k_{EXP}	k_{LIT}
cis-3-Hexen-1-ol (100)	H_3O^+ (19)	$C_6H_{11}^+$ (83) $C_6H_{11}OH_2^+$ (101) Other	95 4 1	2.9	3.3	3.2[5], 2.8[43]
	$H_3O^+\cdot H_2O$ (37)	$C_6H_{11}^+$ (83) $C_6H_{11}OH_2^+$ (101) $C_6H_{11}OH_2^+\cdot H_2O$ (119)	12 33 55	2.3	2.3	2.7[5]
	$H_3O^+\cdot(H_2O)_2$ (55)	$C_6H_{11}OH_2^+\cdot H_2O$ (119) $C_6H_{11}OH_2^+\cdot(H_2O)_2$ (137) Other	80 18 2	2.0	2.2	N/A
	$H_3O^+\cdot(H_2O)_3$ (73)	$C_6H_{11}OH_2^+\cdot(H_2O)_2$ (137) $C_6H_{11}OH_2^+\cdot(H_2O)_3$ (155)	75 25	1.8	1.8	N/A
trans-2-Hexen-1-ol (100)	H_3O^+ (19)	$C_6H_{11}^+$ (83) Other	99 1	2.8	2.7	3.3[5], ~3[43]
	$H_3O^+\cdot H_2O$ (37)	$C_6H_{11}^+$ (83) Other	99 1	2.1	2.4	2.6[5]
	$H_3O^+\cdot(H_2O)_2$ (55)	$C_6H_{11}OH_2^+\cdot H_2O$ (119) $C_6H_{11}OH_2^+\cdot(H_2O)_2$ (137)	42 57	1.9	2.5	N/A
	$H_3O^+\cdot(H_2O)_3$ (73)	$C_6H_{11}^+$ (83) $C_6H_{11}OH_2^+\cdot(H_2O)_2$ (137) $C_6H_{11}OH_2^+\cdot(H_2O)_3$ (155)	5 90 5	1.7	1.9	N/A

Table 6
Reactions of C_5 compounds with the respective product ions of H_3O^+/C_5 reactions.

Neutral reactant	Reactant ion	Product ion distribution		Reaction rates constants (10^{-9} cm^3 molecule^{-1} s^{-1})	
		Product ions	(%)	k_{COL}	k_{EXP}
2-Methyl-3-buten-2-ol (86)	$C_5H_9^+$ (69)	$C_6H_9^+$ (81)	24	1.7	1.3
		$C_{10}H_{17}^+$ (137)	64		
		$C_5H_9^+ \cdot C_5H_9OH$ (155)	8		
		Other	4		
	$C_5H_9OH_2^+$ (87)	$C_5H_9OH_2^+ \cdot H_2O$ (105)	7	1.6	1.5
		$C_5H_9^+ \cdot C_5H_9OH$ (155)	92		
		Other	1		
	$C_2H_5O^+$[a] (45)	$C_5H_9^+$ (69)	100	2.1	1.9
1-Penten-3-ol (86)	$C_5H_9^+$ (69)	$C_6H_9^+$ (81)	8	1.7	0.47
		$C_6H_{13}^+$ (85)	6		
		$C_7H_{11}^+$ (95)	5		
		$C_8H_{15}^+$ (111)	2		
		$C_{10}H_{17}^+$ (137)	54		
		$C_5H_9^+ \cdot C_5H_9OH$ (155)	20		
		Other	5		
	$C_5H_9OH_2^+$ (87)	$C_5H_9OH_2^+ \cdot H_2O$ (105)	15	1.6	1.5
		$C_5H_9^+ \cdot C_5H_9OH$ (155)	29		
		$(C_5H_9OH)_2H^+$ (173)	51		
		Other	5		

[a] Count rate 150 cps, 100% pure.

nation (reaction (18)).

$$C_5H_9OH + H_3O^+ \cdot (H_2O)_3 \rightarrow C_5H_9OH_2^+ \cdot (H_2O)_2 + 2H_2O \quad (18)$$

3.2.2. Reactions with cis-3-hexen-1-ol and trans-2-hexen-1-ol

As can be seen in Table 5, the experimental rate constant values of the H_3O^+/C_6 reactions agree well with previously measured values and with the calculated collision rate constants, indicating that these reactions also take place at every collision.

The H_3O^+/*cis*-3-hexen-1-ol reaction is found to proceed for 95% via dissociative proton transfer with elimination of a water molecule, resulting in a $C_6H_{11}^+$ fragment (reaction (22a)), and for 4% via non-dissociative proton transfer (reaction (19b)). Custer et al. also reported minor fragment ions at *m*/*z* 67 and 99 for this reaction but neither of these have been observed in the present study. The ion at *m*/*z* 99 ($C_7H_{15}^+$) they observed can possibly be attributed to secondary ion chemistry since it has been detected when measuring the secondary reaction of protonated *cis*-3-hexen-1-ol with *cis*-3-hexen-1-ol (see Section 3.3.2).

The H_3O^+/*trans*-2-hexen-1-ol reaction leads to 99% $C_6H_{11}^+$ formation as a result of proton transfer followed by ejection of a H_2O molecule (reaction (19a)).

$$C_6H_{11}OH + H_3O^+ \rightarrow C_6H_{11}^+ + 2H_2O \quad (19a)$$

$$C_6H_{11}OH + H_3O^+ \rightarrow C_6H_{11}OH_2^+ + H_2O \quad (19b)$$

A large difference was observed between $H_3O^+ \cdot H_2O$ reactions with *cis*-3-hexen-1-ol and *trans*-2-hexen-1-ol. The $H_3O^+ \cdot H_2O$/*cis*-3-hexen-1-ol reaction proceeds for 12% via dissociative proton transfer resulting in a $C_6H_{11}^+$ fragment (reaction (20a)), for 33% via non-dissociative proton transfer (reaction (20b)) and for 55% via ligand switching (reaction (20c)). In contrast with these results, the $H_3O^+ \cdot H_2O$/*trans*-2-hexen-1-ol reaction was found to almost exclusively proceed via dissociative proton transfer (reaction (20a)).

$$C_6H_{11}OH + H_3O^+ \cdot H_2O \rightarrow C_6H_{11}^+ + 3H_2O \quad (20a)$$

$$C_6H_{11}OH + H_3O^+ \cdot H_2O \rightarrow C_6H_{11}OH_2^+ + 2H_2O \quad (20b)$$

$$C_6H_{11}OH + H_3O^+ \cdot H_2O \rightarrow C_6H_{11}OH_2^+ \cdot H_2O + H_2O \quad (20c)$$

The $H_3O^+ \cdot (H_2O)_2$ reactions were found to proceed mainly via ligand switching (reaction (21c)) and ligand switching with H_2O elimination (reaction (21b)). However, for *trans*-2-hexen-1-ol a small contribution of the proton transfer product (4%, reaction (21a)) was also observed.

$$C_6H_{11}OH + H_3O^+ \cdot (H_2O)_2 \rightarrow C_6H_{11}OH_2^+ + 3H_2O \quad (21a)$$

$$C_6H_{11}OH + H_3O^+ \cdot (H_2O)_2 \rightarrow C_6H_{11}OH_2^+ \cdot H_2O + 2H_2O \quad (21b)$$

$$C_6H_{11}OH + H_3O^+ \cdot (H_2O)_2 \rightarrow C_6H_{11}OH_2^+ \cdot (H_2O)_2 + H_2O \quad (21c)$$

The $H_3O^+ \cdot (H_2O)_3$ reactions were found to proceed mainly via ligand switching followed by H_2O elimination (reaction (22b)). The ligand switching product was also observed for both compounds. Also, for *trans*-2-hexen-1-ol a small contribution of the $C_6H_{11}^+$ fragment (4%, reaction (22a)) was observed.

$$C_6H_{11}OH + H_3O^+ \cdot (H_2O)_3 \rightarrow C_6H_{11}^+ + 5H_2O \quad (22a)$$

$$C_6H_{11}OH + H_3O^+ \cdot (H_2O)_3 \rightarrow C_6H_{11}OH_2^+ \cdot (H_2O)_2 + 2H_2O \quad (22b)$$

$$C_6H_{11}OH + H_3O^+ \cdot (H_2O)_3 \rightarrow C_6H_{11}OH_2^+ \cdot (H_2O)_3 + H_2O \quad (22c)$$

3.3. Secondary reactions

The reactions of 2-methyl-3-buten-2-ol, 1-penten-3-ol, *cis*-3-hexen-1-ol and *trans*-2-hexen-1-ol with their respective product ions resulting from reactions with H_3O^+ reactant ions have been investigated in order to assess the influence of possible secondary ion chemistry on CIMS detection of these reactive neutrals in case large amounts of these compounds would be present in the reactor. In addition, the reactions of these product ions with H_2O vapour have been studied in order to evaluate the influence of humidity in the CIMS reactor. The product ions used had a purity of at least 98.5% and a count rate of at least 600 cps unless otherwise indicated.

3.3.1. Reactions of product ions of H_3O^+/neutral reactions with the associated neutral

3.3.1.1. Reactions with 2-methyl-3-buten-2-ol and 1-penten-3-ol. In Table 6, the reaction rate constants and product ion distributions for the secondary reactions with C_5 compounds are presented. The $C_5H_9^+$/2-methyl-3-buten-2-ol and the $C_5H_9^+$/1-penten-3-ol reaction were found to have a reaction efficiency of 76% and 28%, respectively. The fact that only $C_5H_9^+$ ions at *m*/*z* 69 were injected in

Table 7
Reactions of C_6 compounds with the product ions of the respective H_3O^+/C_6 reactions.

Neutral reactant	Reactant ion	Product ion distribution		Reaction rates constants (10^{-9} cm^3 molecule^{-1} s^{-1})	
		Product ions	(%)	k_{COL}	k_{EXP}
cis-3-Hexen-1-ol (100)	$C_6H_{11}^+$	$C_7H_{15}^+$ (99)	2	1.7	0.83
		$C_6H_{11}OH_2^+$ (101)	4		
		$C_{10}H_{19}^+$ (139)	2		
		$C_{12}H_{21}^+$ (165)	5		
		$C_6H_{11}^+ \cdot C_6H_{11}OH$ (183)	86		
		Other	1		
	$C_6H_{11}OH_2^+$[a]	$(C_6H_{11}OH)_2H^+$ (201)	100	1.6	1.6
trans-2-Hexen-1-ol (100)	$C_6H_{11}^+$	$C_6H_9^+$ (81)	11	1.6	1.2
		$C_7H_{15}^+$ (99)	2		
		$C_8H_{13}^+$ (109)	4		
		$C_{12}H_{21}^+$ (165)	74		
		$C_6H_{11}^+ \cdot C_6H_{11}OH$ (183)	7		
		Other	2		

[a] Count rate 350 cps, 100% pure.

the reactor and that the isotope at *m*/*z* 70 was detected as a product ion of these reactions reveals the presence of a hidden channel.

The $C_5H_9OH_2^+$/2-methyl-3-buten-2-ol, $C_5H_9OH_2^+$/1-penten-3-ol and $C_2H_5O^+$/1-penten-3-ol reactions were found to take place at the collision rate.

The $C_2H_5O^+$/1-penten-3-ol reaction results in a single $C_5H_9^+$ product ion (reaction (23)):

$$C_2H_5O^+ + \text{1-penten-3-ol} \rightarrow C_5H_9^+ + \text{neutrals} \quad (23)$$

For the $C_5H_9^+/C_5H_9OH$ reactions, the association product $C_5H_9^+ \cdot C_5H_9OH$ (reaction (24a)), the H_2O eliminated association product $C_{10}H_{17}^+$ (reaction (24b)) and some other fragment ions have been observed. Only the reaction with 1-penten-3-ol resulted in a $C_6H_9^+$ fragment (reaction (24c)).

$$C_5H_9^+ + C_5H_9OH \xrightarrow{M} C_5H_9^+ \cdot C_5H_9OH \quad (24a)$$

$$C_5H_9^+ + C_5H_9OH \rightarrow C_{10}H_{17}^+ + H_2O \quad (24b)$$

$$C_5H_9^+ + C_5H_9OH \rightarrow C_6H_9^+ + \text{neutrals} \quad (24c)$$

The association product $(C_5H_9OH)_2H^+$ (reaction (25a)) and fragment ions resulting from elimination of one and two water molecules from the association product (reactions (25b), (25c)) were found for the $C_5H_9OH_2^+$/1-penten-3-ol reaction. However, for the $C_5H_9OH_2^+$/2-methyl-3-buten-2-ol reaction, no association product was found.

$$C_5H_9OH_2^+ + C_5H_9OH \xrightarrow{M} (C_5H_9OH)_2H^+ \quad (25a)$$

$$C_5H_9OH_2^+ + C_5H_9OH \rightarrow C_5H_9^+ \cdot C_5H_9OH + H_2O \quad (25b)$$

$$C_5H_9OH_2^+ + C_5H_9OH \rightarrow C_{10}H_{17}^+ + 2H_2O \quad (25c)$$

3.3.1.2. Reactions with cis-3-hexen-1-ol and trans-2-hexen-1-ol. In Table 7, the rate constants and product ion distributions for the secondary reactions with C_6 compounds are presented. In analogy with the $C_5H_9^+/C_5$ reactions, the $C_6H_{11}^+$/*cis*-3-hexen-1-ol and $C_6H_{11}^+$/*trans*-2-hexen-1-ol reactions were also found to occur with a limited reaction efficiency of 49% and 75%, respectively. The presence of a hidden proton transfer channel was observed for the *trans*-2-hexen-1-ol reaction by the presence of the $C_6H_{11}^+$ isotope at *m*/*z* 84 when injecting the isotope at *m*/*z* 83.

The $C_6H_{11}OH_2^+$/*cis*-3-hexen-1-ol reaction was found to proceed at the collision rate.

The $C_6H_{11}^+$/*cis*-3-hexen-1-ol reaction resulted mainly in the formation of the association product (reaction (26a)). Other pathways include the elimination of a H_2O molecule (reaction (26b)) and a minor proton transfer channel (reaction (26c)).

$$C_6H_{11}^+ + \textit{cis}\text{-3-hexen-1-ol} \xrightarrow{M} C_6H_{11}^+ \cdot C_6H_{11}OH \quad (26a)$$

$$C_6H_{11}^+ + \textit{cis}\text{-3-hexen-1-ol} \rightarrow C_{12}H_{21}^+ + H_2O \quad (26b)$$

$$C_6H_{11}^+ + \textit{cis}\text{-3-hexen-1-ol} \rightarrow C_6H_{11}OH_2^+ + \text{neutrals} \quad (26c)$$

In contrast, the $C_6H_{11}^+$/*trans*-2-hexen-1-ol reaction has only a minor association product channel (reaction (27a)) and the fragment ion resulting from water elimination has the largest contribution (reaction (27b)). A $C_6H_9^+$ fragment with a considerable yield has also been observed (reaction (27c)). No proton transfer product ion has been detected for this reaction.

$$C_6H_{11}^+ + \textit{trans}\text{-2-hexen-1-ol} \xrightarrow{M} C_6H_{11}^+ \cdot C_6H_{11}OH \quad (27a)$$

$$C_6H_{11}^+ + \textit{trans}\text{-2-hexen-1-ol} \rightarrow C_{12}H_{21}^+ + H_2O \quad (27b)$$

$$C_6H_{11}^+ + \textit{trans}\text{-2-hexen-1-ol} \rightarrow C_6H_9^+ + \text{neutrals} \quad (27c)$$

The $C_6H_{11}OH_2^+$/*cis*-3-hexen-1-ol reaction was found to proceed exclusively by association (reaction (28)).

$$C_6H_{11}OH_2^+ + \textit{trans}\text{-2-hexen-1-ol} \xrightarrow{M} (C_6H_{11}OH)_2H^+ \quad (28)$$

3.3.2. Hydration of H_3O^+/C_5 and H_3O^+/C_6 product ions

The termolecular rate constants for the hydration reactions of the H_3O^+/C_5 and H_3O^+/C_6 product ions have been measured and the results are listed in Table 8. The absence of hydration of the $C_5H_9^+$ and $C_6H_{11}^+$ ions is consistent with previous observations involving pure hydrocarbon ions [3,26,45]. The oxygen-bearing product

Table 8
Termolecular hydration rate constant of H_3O^+/C_5 and H_3O^+/C_6 product ions. NR: no reaction observed.

Parent neutral	Reactant ion	Reaction rate constants (10^{-27} cm^6 s^{-1})
2-Methyl-3-buten-2-ol	$C_5H_9^+$	NR
	$C_5H_9OH_2^+$	4.8
1-Penten-3-ol	$C_2H_5O^+$	1.9
	$C_5H_9^+$	NR
	$C_5H_9OH_2^+$	4.5
cis-3-Hexen-1-ol	$C_6H_{11}^+$	NR
	$C_6H_{11}OH_2^+$	7.3
trans-2-Hexen-1-ol	$C_6H_{11}^+$	NR

ions, however, were all found to hydrate much faster than the CIMS reactant H_3O^+ ion.

4. Conclusions

Our newly developed tandem FA-SIFT instrument has been validated by studying the reactions of methanol and ethanol with a series of reactant ions.

Injection of a sufficiently high current of the more weakly bound $H_3O^+{\cdot}H_2O$ clusters was highly successful and by breaking-up $H_3O^+{\cdot}(H_2O)_3$ ions in the SIFT injector system, 90% pure $H_3O^+{\cdot}(H_2O)_2$ ion swarms could be created in the SIFT reactor. Clean introduction of $H_3O^+{\cdot}(H_2O)_3$ ions in the reactor was not possible, but $H_3O^+{\cdot}(H_2O)_3$ reactions could nevertheless be studied in the presence of $H_3O^+{\cdot}(H_2O)_2$ ions, resulting from partial break-up of $H_3O^+{\cdot}(H_2O)_3$ in the SIFT injector.

For the majority of the reactions studied, the rate constants and product ion distributions were found to be in good agreement with available literature data.

Weakly bound cluster product ions such as $CH_3OH_2^+{\cdot}(H_2O)_2$ and $C_2H_5OH_2^+{\cdot}(H_2O)_2$ were found to survive sampling into the detection mass spectrometer section, indicating that the electric field and the residual pressure in the region behind the inlet orifice are sufficiently low to avoid collision-induced dissociation of these ions, which would affect product ion distributions.

The data on ion/molecule reactions involving C_5 and C_6 biogenic alcohols lead to a better insight into the ion chemistry that takes place in a medium-pressure CIMS reactor when these reactant neutrals and water vapour are simultaneously present in the reactor while introducing H_3O^+ reactant ions. $H_3O^+{\cdot}(H_2O)_n$ (n = 0–3) ions were found to react at the collision rate with the four unsaturated biogenic alcohols studied, resulting in $C_5H_9^+{\cdot}(H_2O)_m$ (m = 0–2) and $C_6H_{11}^+{\cdot}(H_2O)_m$ (m = 0–3) product ions for the pentenols and hexenols, respectively. No major differences in the main reaction mechanisms were found for isomeric species, except for the reactions of $H_3O^+{\cdot}H_2O$ with *cis*-3-hexen-1-ol and *trans*-2-hexen-1-ol. Whereas the first reaction proceeds by ligand switching, proton transfer and water elimination following proton transfer, the latter proceeds entirely by water elimination following proton transfer.

The final $C_5H_9^+{\cdot}(H_2O)_m$ ($m > 0$) and $C_6H_{11}^+{\cdot}(H_2O)_m$ ($m > 0$) distribution at the downstream end of the SIFT reactor will depend on further hydration of the product ions, which was found to be fast for the protonated alcohols, and on the mass-dependent diffusion of the product ions in the He buffer gas flow.

The $H_3O^+{\cdot}(H_2O)_n$/pentenol (n = 0–2) and $H_3O^+{\cdot}(H_2O)_n$/hexenol (n = 0–2) rate constants that were obtained in this work can serve as input to Eq. (11) in Ref. [8] for a more accurate SIFT-MS quantification of these species in moist conditions.

When decreasing the drift field in a PTR-MS reactor the contribution of $H_3O^+{\cdot}H_2O$, and to a lesser extent, $H_3O^+{\cdot}(H_2O)_2$, to the reactant ion distribution can become important and therefore, characterization of the reactions of $H_3O^+{\cdot}(H_2O)_n$ (n = 0–2) with the biogenic alcohols is also important for quantification of these neutral reactants with the PTR-MS technique. However, it should be noticed that the FA-SIFT ion/molecule reaction studies, which are performed at true thermal conditions, only give an indication of which product ions can be expected in the PTR-MS in which the reactant ions gain additional energy from the presence of an electric field.

Finally, when introducing relatively large amounts of biogenic alcohols ROH in a CIMS reactor, secondary reactions between $H_3O^+{\cdot}(H_2O)_n$/ROH product ions and ROH can take place and these will have to be taken into account as well for accurate quantification. By studying the reactions of H_3O^+/ROH product ions with ROH (for the two pentenols and the two hexenols), new kinetic and mechanistic information for these reactions has been obtained.

Acknowledgements

This research was supported by the Institute for the Promotion of Innovation through Science and Technology in Flanders (IWT-Vlaanderen) and by the Belgian Federal Science Policy Office (Project # MO/35/022).

References

[1] A. Guenther, C.N. Hewitt, D. Erickson, R. Fall, C. Geron, T. Graedel, P. Harley, L. Klinger, M. Lerdau, W.A. McKay, T. Pierce, B. Scholes, R. Steinbrecher, R. Tallamraju, J. Taylor, P. Zimmerman, J. Geophys. Res. 100 (1995) 8873.
[2] N. Schoon, C. Amelynck, L. Vereecken, E. Arijs, Int. J. Mass Spectrom. 229 (2003) 231.
[3] F. Dhooghe, C. Amelynck, N. Schoon, E. Debie, P. Bultinck, F. Vanhaecke, Int. J. Mass Spectrom. 272 (2008) 137.
[4] C. Amelynck, N. Schoon, T. Kuppens, P. Bultinck, E. Arijs, Int. J. Mass Spectrom. 147 (2005) 1.
[5] N. Schoon, C. Amelynck, E. Debie, P. Bultinck, E. Arijs, Int. J. Mass Spectrom. 263 (2007) 127.
[6] M. Demarcke, C. Amelynck, N. Schoon, F. Dhooghe, H. Van Langenhove, J. Dewulf, Int. J. Mass Spectrom. 279 (2009) 156.
[7] D. Smith, P. Španěl, Int. Rev. Phys. Chem. 15 (1996) 231.
[8] D. Smith, P. Španěl, Mass Spectrom. Rev. 24 (2005) 661.
[9] W. Lindinger, A. Hansel, A. Jordan, Int. J. Mass Spectrom. Ion Process. 73 (1998) 191.
[10] J. de Gouw, C. Warneke, Mass Spectrom. Rev. 26 (2007) 223.
[11] E.C. Fortner, W.B. Knighton, Rapid Commun. Mass Spectrom. 22 (2008) 2597.
[12] D. Smith, N.G. Adams, Adv. At. Mol. Phys. 24 (1988) 1.
[13] D. Smith, N.G. Adams, J. Phys. D: Appl. Phys. 13 (1980) 1267.
[14] G.I. Mackay, G.D. Vlachos, D.K. Bohme, H.I. Schiff, Int. J. Mass Spectrom. Ion Phys. 36 (1980) 259.
[15] J.M. Van Doren, S.E. Barlow, C.H. Depuy, V.M. Bierbaum, Int. J. Mass Spectrom. Ion Process. 81 (1987) 85.
[16] T. Karl, R. Fall, A. Jordan, W. Lindinger, Atmos. Environ. 35 (2001) 3905.
[17] P.C. Harley, V. Fridd-Stroud, J. Greenberg, A. Guenther, P. Vasconellos, J. Geophys. Res. 103 (1998) 25479.
[18] N.G. Adams, D. Smith, Int. J. Mass Spectrom. Ion Phys. 21 (1976) 349.
[19] Y.K. Lau, S. Ikuta, P. Kebarle, J. Am. Chem. Soc. 104 (1982) 1462.
[20] Y. Ikezoe, S. Matsuoka, M. Takebe, A. Viggiano, Gas Phase Ion-Molecule Reaction Rate Constants through 1986, Maruzen Company Ltd., Tokyo, 1987.
[21] P. Španěl, D. Smith, J. Am. Soc. Mass Spectrom. 12 (2001) 863.
[22] T. Su, W.J. Chesnavich, J. Chem. Phys. 76 (1982) 5183.
[23] T. Su, J. Chem. Phys. 89 (1988) 5355.
[24] D.R. Lide (Ed.), CRC Handbook of Chemistry and Physics, CRC, Boca Raton, 1991.
[25] F.C. Fehsenfeld, I. Dotan, D.L. Albritton, C.J. Howard, E.E. Ferguson, J. Geophys. Res. 83 (1978) 1333.
[26] P. Španěl, D. Smith, J. Phys. Chem. 99 (1995) 15551.
[27] P. Španěl, D. Smith, Int. J. Mass Spectrom. Ion Process. 167–168 (1997) 375.
[28] G.I. Mackay, S.D. Tanner, A.C. Hopkinson, D.K. Bohme, Can. J. Chem. 57 (1979) 1518.
[29] H.S. Lee, M. Drucker, N.G. Adams, Int. J. Mass Spectrom. Ion Process. 117 (1992) 101.
[30] D.K. Böhme, G.I. Mackay, S.D. Tanner, J. Am. Chem. Soc. 101 (1979) 3724.
[31] R.A. Morris, A.A. Viggiano, J.F. Paulson, M.J. Henchman, J. Am. Chem. Soc. 113 (1991) 5932.
[32] L.M. Bass, R.D. Cates, M.F. Jarrold, N.J. Kirchner, M.T. Bowers, J. Am. Chem. Soc. 105 (1983) 7024.
[33] T.D. Fridgen, J.D. Keller, T.B. McMahon, J. Phys. Chem. A 105 (2001) 3816.
[34] T.B. McMahon, J.L. Beauchamp, J. Phys. Chem. 81 (1977) 593.
[35] Z. Karpas, M. Meot-ner, J. Phys. Chem. 93 (1989) 1549.
[36] T.T. Dang, V.M. Bierbaum, Int. J. Mass Spectrom. Ion Process. 117 (1992) 65.
[37] M. Meot-ner (Mautner), J. Am. Chem. Soc. 106 (1984) 1265.
[38] E.P. Hunter, S.G. Lias, J. Phys. Chem. Ref. Data 27 (1998) 413.
[39] P. Kebarle, Annu. Rev. Phys. Chem. 28 (1977) 445.
[40] T.D. Fridgen, T.B. McMahon, J. Phys. Chem. A 106 (2002) 9648.
[41] P. Španěl, D. Smith, Rapid Commun. Mass Spectrom. 14 (2000) 1898.
[42] V.M. Bierbaum, M.F. Golde, F. Kaufman, J. Chem. Phys. 65 (1976) 2715.
[43] T.G. Custer, S. Kato, R. Fall, V.M. Bierbaum, Int. J. Mass Spectrom. 223–224 (2003) 427.
[44] E. Michel, N. Schoon, C. Amelynck, C. Guimbaud, V. Catoire, E. Arijs, Int. J. Mass Spectrom. 244 (2005) 50.
[45] D. Smith, A.M. Diskin, Y. Ji, P. Španěl, Int. J. Mass Spectrom. 209 (2001) 81.